Electronic Supplementary Material (ESI) for ChemComm. This journal is © The Royal Society of Chemistry 2021

Supporting Information for

Ultrafine Co_6W_6C as an Efficient Anode Catalyst for Direct Hydrazine Fuel Cells

Mengrui Zhang, Jianping Zhu, Bin Liu, Yongkang Hou, Chao Zhang, * Jingping Wang, and Jingyang Niu*

Henan Key Laboratory of Polyoxometalate Chemistry, Institute of Molecular and Crystal Engineering, College of Chemistry and Chemical Engineering, Henan University, Kaifeng, Henan 475004, P. R. China

Fax: (+ 86)371-23886876
E-mail: zhangchao@henu.edu.cn; jyniu@henu.edu.cn

Results and Discussion

1. Characterization data (**Fig. S1-S35**)

2. Tables results (**Table S1-S2**)

Experimental Section

Chemicals and Reagents.

All chemicals were obtained from commercial suppliers and used without further purification unless specified otherwise: zinc nitrate hexahydrate (99%, AR), 2-methylimidazole (2-mIm, 98%, AR), Triethylamine (TEA, 99%, AR), potassium hydroxide (85%, AR), Hydrazine hydrate (80%, AR), carbon black (EC600JD), 5 wt% Nafion solution.

Characterization

X-ray power diffraction (XRD) was measured on a Bruker D8 Advance X-ray diffractometer equipped with graphite monochromatized Cu Kα radiation (λ = 1.54 Å). Liquid ultraviolet-visible (UV-vis) spectra were operated on UV-4100 spectrometer. Infrared (IR) spectra were performed on a PerkinElmer spectrum instrument with KBr tabletting, and the range was 400-4500 cm^{-1}. Scanning electron microscopy (SEM) images were carried on JSM-7610F. Transmission electron microscopy (TEM) images were carried out on JEM-2100 with electron energy of 200 kV. N_2 sorption isotherm was operated on Quadrasorb SI-4; Brunauer-Emmett-Teller (BET) surface area and pore size were analyzed using the ASiQwin software.

Electrochemical measurements

All electrochemical experiments were conducted on the CHI 660e electrochemical station in a standard three electrode cell at room temperature. A glassy carbon electrode (GC, diameter = 5mm), an Ag/AgCl electrode (3.5 M KCl), and a carbon rod were used as the working electrode, reference electrode and counter electrode, respectively. The reference electrode was placed in a position very close to the working electrode.

5 mg of the catalysts were dispersed in a mixture of ethanol (0.48 mL) and 5wt% Nafion (0.02

mL) by sonication to form a homogeneous ink. Typically, 10 μL well-dispersed catalysts (corresponding to a catalyst loading of 0.51 mg cm^{-2}) were covered on the GC electrode and then dried in an ambient environment for measurements. Cyclic voltammetry curves were tested in alkaline solution with a scan rate of 5 mV s^{-1}. The Chronoamperometry were tested at a fixed potential vs RHE (HzOR: 0.8 V). The potential vs RHE was converted to RHE via the Nernst equation: $E_{RHE} = E_{Ag/AgCl} + 0.059pH + E^{\theta}_{Ag/AgCl}$

Due to the strong magnetic properties of Co-ZIF-8/C-p samples, TEM tests cannot be performed. To determine the size of Co particles, we use the Sherrer equation to estimate the Co's size on jade software (average particle size 3-5 nm):

$$D=k\lambda/\beta\cos\theta$$

D: grain size; k: index, 1.0; λ: X-ray wavelength; β: full width at half maxima, FWHM; θ: angle of deviation.

Turnover frequency (TOF)

The calculation of TOF was based on a previous standard method in electrocatalytic hydrazine oxidation reaction field.[1] The values of TOF were calculated by assuming that all metal atoms are involved in the catalytic processes, which all represent the lowest limits of the models. The values of TOF (e $site^{-1}$ h^{-1}) were calculated using the following equation:

$$TOF = j*S_{GEO}/(F*n)$$

Where *j* (mA cm^{-2}) is the as-measured current density at various potential, S_{GEO} (0.19625 cm^{-2}) represents the surface area of the glassy carbon electro, F is the Faraday constant (96485 C mol^{-1}), and n is the moles of metal atoms on the electrode, the moles of Co_6W_6C for Co_6W_6C@C can be calculated by the loading weight of catalysts and ICP results.

Determination of Faradaic efficiency

Faradaic efficiency (FE) of Co_6W_6C@C catalyst is defined as the ratio of the amount of experimentally determined N_2 to that of the theoretically expected N_2 from the hydrazine oxidation reaction. The

nitrogen (N_2) product was analyzed by gas chromatography. The standard curve for quantitative detection of N_2 was determined by external standard method, and the conditions for the calibration are the same as the conditions for catalytic reaction.

Typically, the solution of 1 M KOH+ 100 mM N_2H_4 was continuously electrolyzed at a fixed potential of 0.6 V (vs RHE) and 1.2 V (vs RHE) for 3.5 h by using Co_6W_6C@C catalyst. The amount of N_2 was determined by gas chromatography at stipulated times (10, 20, 30, 60, 90, 120, 150, 180 and 210 min).

Preparation of oxygen (O_2)-hydrazine fuel cell (O_2-HzFC)

In our O_2-HzFCs, the Co_6W_6C@C NPs supported on Ni foam were directly utilized as anodes with a polymer binder. The cathode catalysts in this work were all prepared according to previous standard method in this field:[2] A mixture of Pt/C (20 wt%, 20 mg), 150 μL Nafion solution (5 wt%), 200 μL deionized water and 1.8 mL isopropanol was sonication for 2 h to form a homogenous dispersion, which was then brushed onto a piece of carbon paper (1.14 cm^{-2}) with a microporous layer. The loading of Pt/C catalyst was 0.6 mg_{Pt} cm^{-2}.

The membrane electrode assembly (MEA) was fabricated by hot-pressing an anode, a cathode, a KOH-doped polybenzimidazole (PBI) membrane, and gasket at 130 ^oC for 10 s. The PBI membrane had been pre-treated with 6 M KOH for 5 h at 80 ^oC, and preserved in deionized water prior to hot-pressing.

The O_2-HzFCs was measured at 80 ^oC on Model 850e fuel cell test system (see **Fig. S28**). The optimized anolyte is 6.0 M KOH + 0.5 M hydrazine hydrate with a flow rate of 1 mL min^{-1} and the catholyte is oxygen with a flow rate of 0.2 L min^{-1}.

Synthesis of samples

α-$Na_{10}[SiW_9O_{34}]\cdot 18H_2O$ (SiW_9)[3] and $K_{10}[SiW_9O_{37}Co_3(H_2O)_3]$ (SiW_9Co_3)[4] were synthesized according to the literature with some modifications.

Synthesis of ZIF-8: The synthesis of ZIF-8 was based on the previous method with some modifications.[5] The 2-methylimidazole (2-mIm, 4.42g, 53.90 mmol) and triethylamine (TEA, 2.95 mL) were dissolved in deionized water (50 mL) with vigorous stirring. A mixture of $Zn(NO_3)_2 \cdot 6H_2O$ (2 g, 6.70 mmol) with 25 mL deionized water was added to the above solution with vigorous stirring for 1 h at room temperature. The resulting white precipitates were collected by centrifuging and washed thoroughly with deionized water for five times. The precipitates were dried in vacuum at 75 °C overnight.

Synthesis of ZIF-8/C (ZIF): The 2-mIm (4.42g, 53.90 mmol), TEA (2.95 mL) and carbon black (0.10 g) were dissolved/dispersed in deionized water (50 mL) with vigorous stirring. A mixture of $Zn(NO_3)_2 \cdot 6H_2O$ (2g, 6.70 mmol) with 25 mL deionized water was added to the above solution with vigorous stirring for 1 h at room temperature. The resulting dark gray precipitates were collected by centrifuging and washed thoroughly with deionized water for five times. The precipitates were dried in vacuum at 75 °C overnight.

Synthesis of SiW_9Co_3@ZIF: The 2-mIm (4.42 g, 53.90 mmol), TEA (2.95 mL) and carbon black (0.10 g) were dissolved/dispersed in deionized water (25 mL) with vigorous stirring. Then, an aqueous solution (20 mL) of $Zn(NO_3)_2 \cdot 6H_2O$ (2 g, 6.70 mmol) and an aqueous solution (20 mL) of SiW_9Co_3 (0.76 g, 0.26 mmol) were simultaneously and slowly added to the above mixture solution with vigorous stirring for 1 h (the molar ratio of SiW_9Co_3: Zn^{2+} =1:25). Gray precipitates were collected by centrifugation and washed with copious water until no SiW_9Co_3 was present in the solution, as evidenced by UV-vis spectroscopy. The product was dried in vacuum at 75 °C overnight.

Synthesis of SiW_9@ZIF: The synthesis of SiW_9@ZIF was similar to SiW_9Co_3@ZIF, except that SiW_9Co_3 was replaced by SiW_9 (0.75 g, 0.26 mmol).

Synthesis of Co-ZIF-8/C: The synthesis of Co-ZIF-8/C was similar to ZIF-8/C, except the $Zn(NO_3)_2 \cdot 6H_2O$ solution was replaced by $Zn(NO_3)_2 \cdot 6H_2O$ (1.71 g, 5.75 mmol)/$Co(NO_3)_2 \cdot 6H_2O$ (0.24 g, 0.81 mmol) mixture solution.

Synthesis of SiW_9Co_3/ZIF: The SiW_9Co_3 (0.72 g) and ZIF-8 (1.28 g) were mixed together and ground uniformly.

Synthesis of SiW_9Co_3/C: SiW_9Co_3 (0.72 g) and amorphous carbon black (0.3 g) were mixed together and ground uniformly.

Synthesis of SiW_9TM_3@ZIF (TM =Fe, Ni, Mn and Cu): Similar to the synthesis procedure of SiW_9Co_3@ZIF, expect that SiW_9Co_3 was replaced by SiW_9Fe_3 (0.73 g, 0.26 mmol), SiW_9Ni_3 (0.76, 0.26 mmol), SiW_9Mn_3 (0.75 g,0.26 mmol), SiW_9Cu_3 (0.76g, 0.26 mmol).

Synthesis of ZIF-8/C-p: The 0.4 g ZIF-8/C composite was transferred into a temperature-programmed furnace under an N_2 flow (40−60 mL min^{-1}), heat-treated at 600 °C for 3 h and then at 900 °C for 4 h with a heating rate of 5 °C min^{-1}. The sample was cooled to room temperature naturally under N_2 flow to obtain ZIF-8/C-p.

Synthesis of Co_6W_6C@C: Similar to the synthesis procedure of ZIF-8/C-p, except the ZIF-8/C was replaced by SiW_9Co_3@ZIF sample. To determine the effect of the calcination temperature on the electrocatalytic performance, the samples were prepared at various temperatures (700, 800, 900, 1000, and 1100 °C)

Synthesis of SiW_9@ZIF-p, Co-ZIF-8/C-p, SiW_9Co_3/ZIF-p, SiW_9Co_3/C-p and SiW_9TM_3@ZIF-

p: Similar to the synthesis procedure of ZIF-8/C-p, except the ZIF-8/C sample was replaced by SiW_9@ZIF, Co-ZIF/8, SiW_9Co_3/ZIF, SiW_9Co_3/C and SiW_9TM_3@ZIF.

Detailed discussions of catalyst synthesis

The Co_6W_6C@C NPs was synthesized by a two-step process: the first step aims to synthesize a Co-, W- and C-containing precursor, and the second step includes a pyrolysis process that converts the precursor into Co_6W_6C NPs. First, SiW_9Co_3 was *in situ* encapsulated into the cavities of ZIF-8 to obtain POM@ZIF precursors (SiW_9Co_3@ZIF). The addition of carbon black aims to increase the carbon content of the precursor so that the precursor can be converted into bimetallic carbides Co_6W_6C in the pyrolysis process. The preparated SiW_9Co_3@ZIF precursor was washed several times to remove adsorbed SiW_9Co_3 on ZIF-8 NP surfaces. No characteristic O→W UV-vis spectroscopy absorption peak was observed in the supernatant solution of the as-synthesized samples (**Fig. S1**), indicating the complete removal of adsorbed SiW_9Co_3 from the ZIF-8 surfaces. The XRD pattern of the preparated sample was in agreement with the simulation results of ZIF-8 (**Fig. S2**), indicating the intactness of the ZIF-8 framework and confirming the absence of crystalline aggregation of SiW_9Co_3. Moreover, the IR spectrum of the preparated sample shows characteristic peaks of SiW_9Co_3 (**Fig. S3**), confirming the presence of SiW_9Co_3 in the as-synthesized samples. Based on these characterizations, we confirm that SiW_9Co_3 clusters have been successfully encapsulated into the cavities of ZIF-8. The as-synthesized sample was denoted as SiW_9Co_3@ZIF hereafter. SEM images of SiW_9Co_3@ZIF suggested that the morphology and size of SiW_9Ni_3@ZIF are similar to those of ZIF nanocrystals (ZIF-8/C) (**Fig. S4&S5**). ICP-AES result showed that the W and Co contents were found to be 20.73 wt% and 2.36 wt%, respectively, in SiW_9Co_3@ZIF (**Table S1**)

Catalytic activities of Co_6W_6C@C for different pyrolysis temperatures

Efforts at optimizing the HzOR catalytic activity of Co_6W_6C@C was further pursued by testing pyrolysis temperatures at 700 °C, 800 °C, 900 °C, 1000 °C, and 1100 °C. As shown in **Fig. S10c** and **S18**, Co_6W_6C@C exhibited the highest HzOR catalytic activity at 900°C, with a maximum current density of 130 mA cm^{-2} at 0.6 V. This peak current density was 2.3, 1.6, 3.3 and 1.8 times greater than those of SiW_9Co_3@ZIF pyrolyzed at 700 °C (57 mA cm^{-2}), 800 °C (82 mA cm^{-2}), 1000 °C (41 mA cm^{-2}) and 1100 °C (71 mA cm^{-2}), respectively. XRD results provided explanations for these catalytic activity differences resulting from the use of different temperatures: as shown in **Fig. S19**, after applying pyrolyses at temperatures of 700 °C and 800 °C, the XRD peaks of the resulting Co_6W_6C samples were very weak, indicating that the crystallization processes did not proceed to completion when carrying out pyrolysis at these low temperatures; after applying pyrolyses at temperatures of 1000 °C and 1100 °C, peaks corresponding to metallic W and Co species appeared in the XRD patterns of the samples, indicating that the ternary carbide Co_6W_6C was over-reduced at high temperatures (**Fig. S20**).

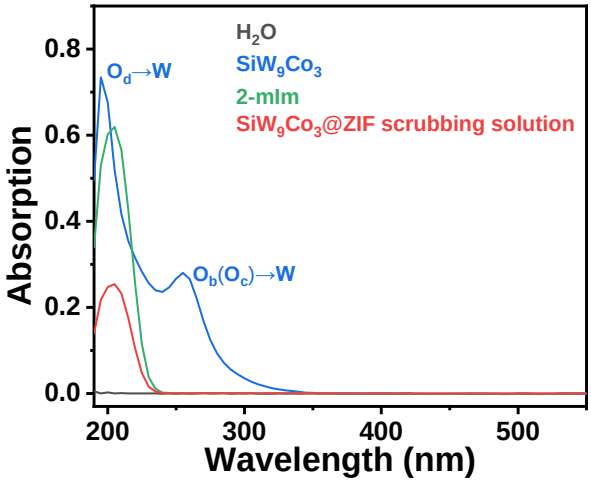

Fig. S1. UV-vis spectra of H_2O, SiW_9Co_3, 2-mIm and SiW_9Co_3@ZIF scrubbing solution.

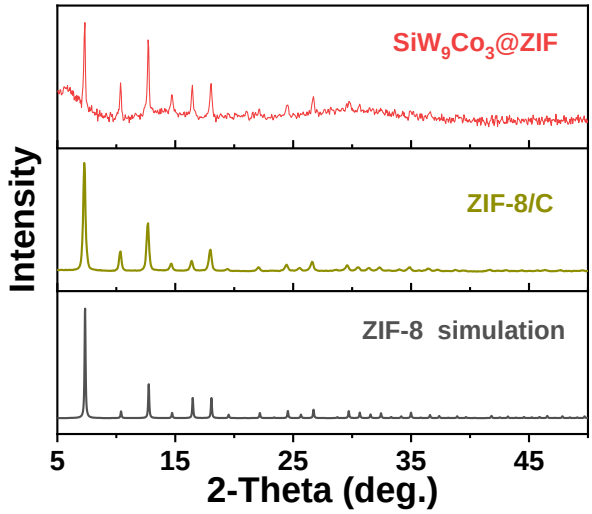

Fig. S2. XRD patterns of ZIF-8 simulation, ZIF-8/C and SiW_9Co_3@ZIF samples.

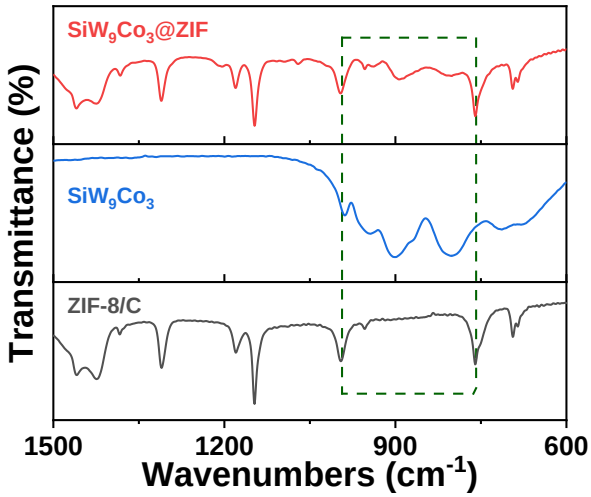

Fig. S3. IR spectra of ZIF-8/C, SiW_9Co_3 and SiW_9Co_3@ZIF samples.

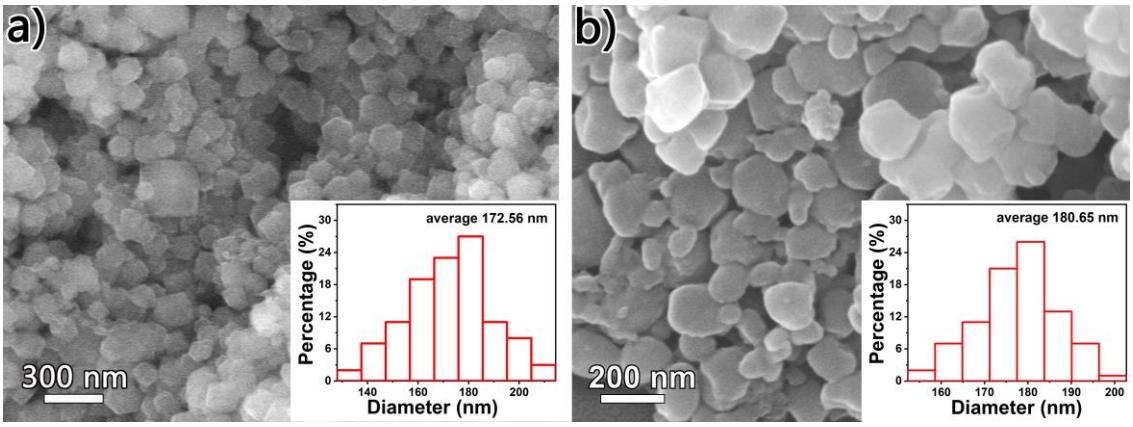

Fig. S4. SEM images of a) ZIF-8/C and b) SiW_9Co_3@ZIF. (inset: particle size distribution of the corresponding samples)

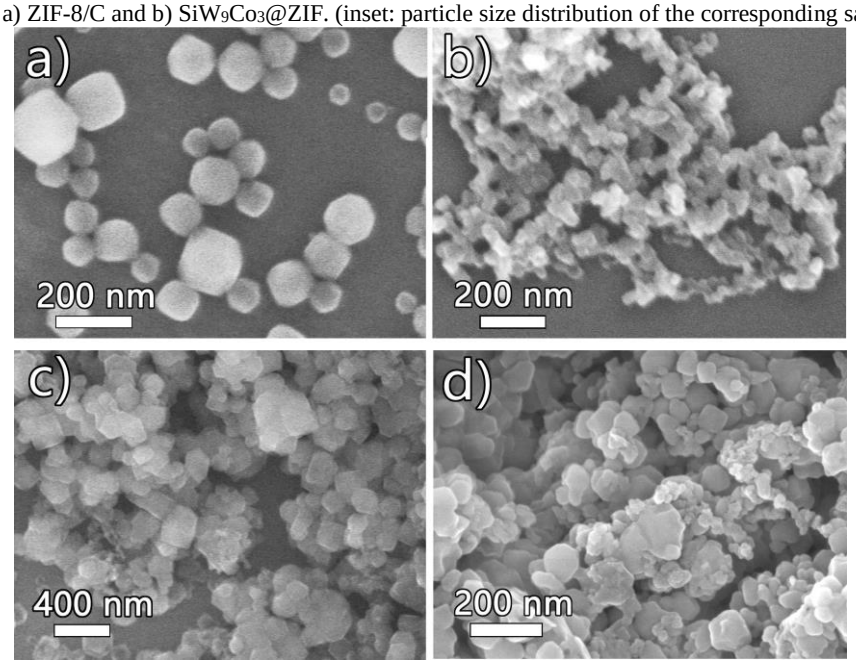

Fig. S5. SEM images of a) ZIF-8, b) carbon black, c) ZIF-8/C and d) SiW_9Co_3@ZIF samples.

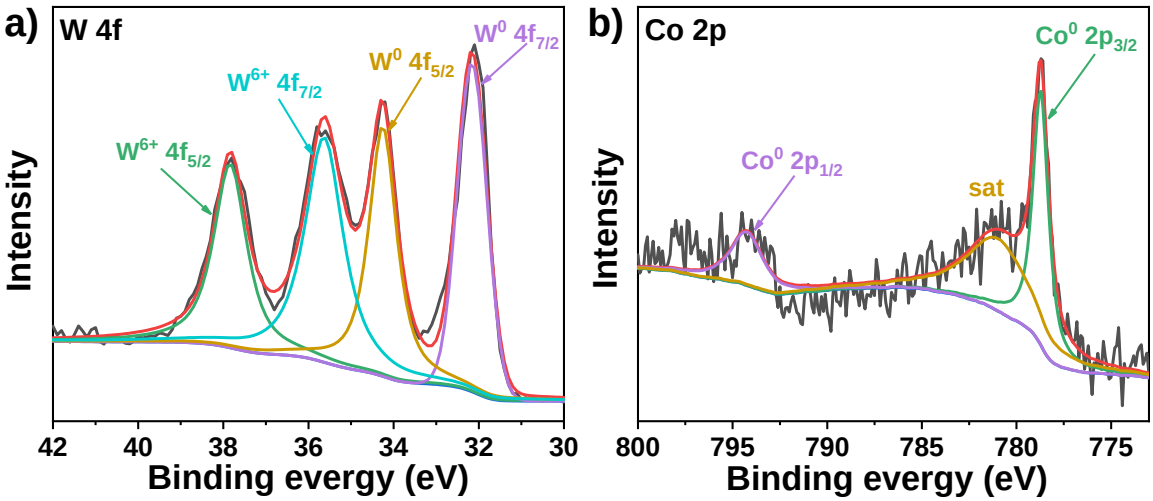

Fig. S6. The high-resolution a) W 4f and b) Co 2p XPS spectra of Co_6W_6C@C.

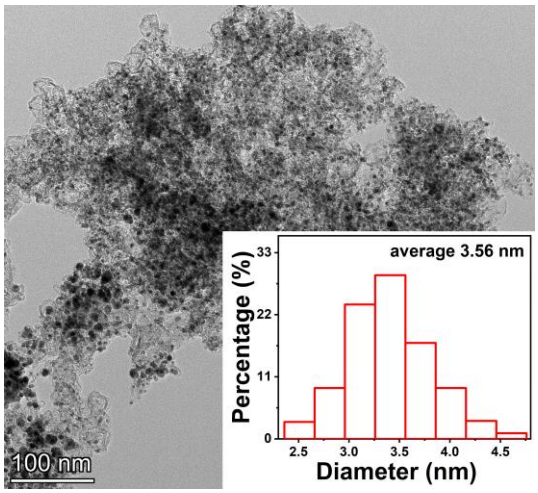

Fig. S7. TEM image of Co_6W_6C@C. (inset: particle size distribution of Co_6W_6C@C)

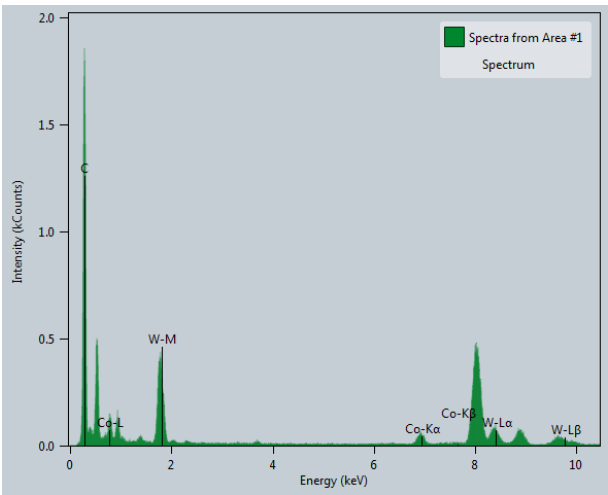

Fig. S8. EDX spectrum of Co_6W_6C@C.

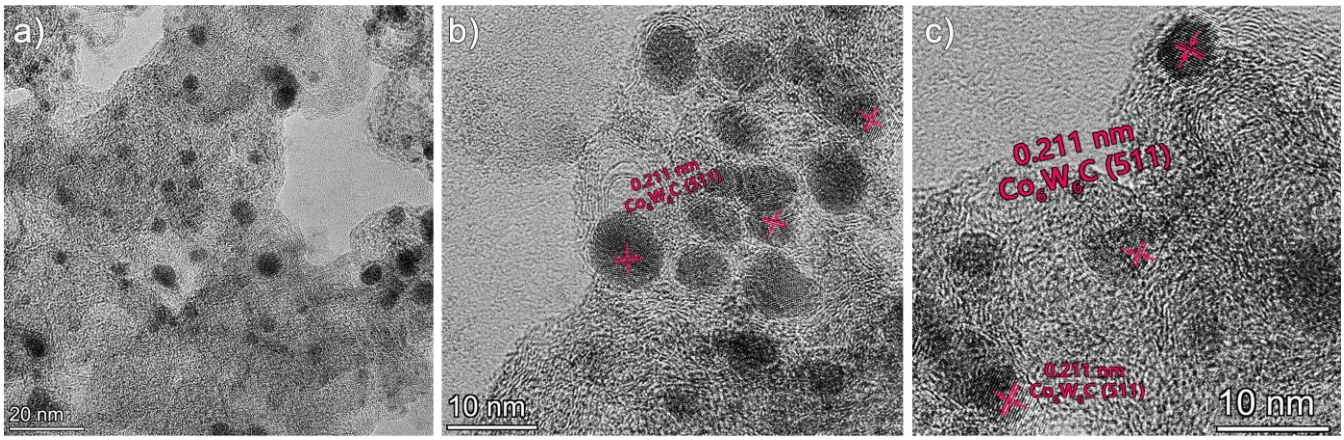

Fig. S9. HRTEM images of Co_6W_6C@C.

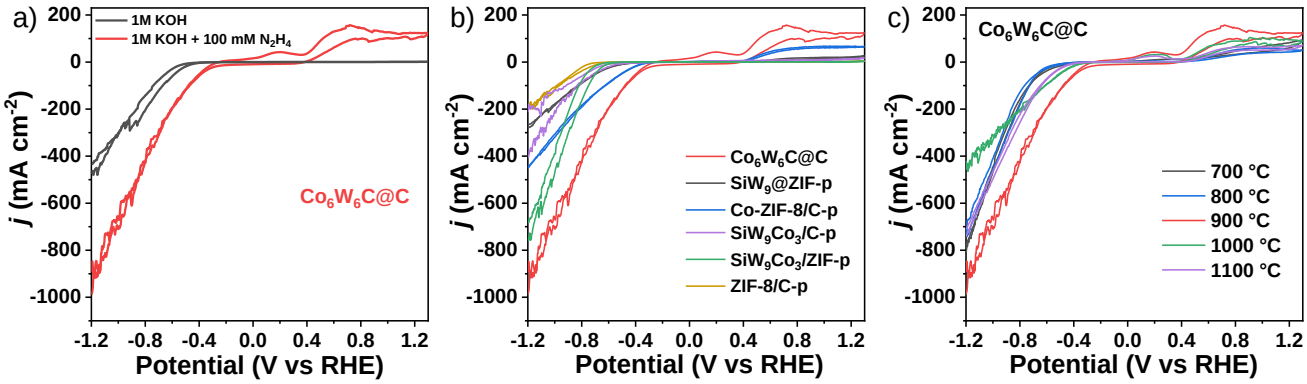

Fig. S10. a) Widened CV curves of a) Co_6W_6C@C in 1 M KOH with and without 100 mM N_2H_4. b) Widened CV curves of different catalysts for HzOR. c) HzOR activities of the Co_6W_6C@C catalyst with different pyrolysis temperatures in 1 M KOH and 100 mM N_2H_4 solution.

Fig. S11. The electrochemical device of HzOR for Co_6W_6C@C.

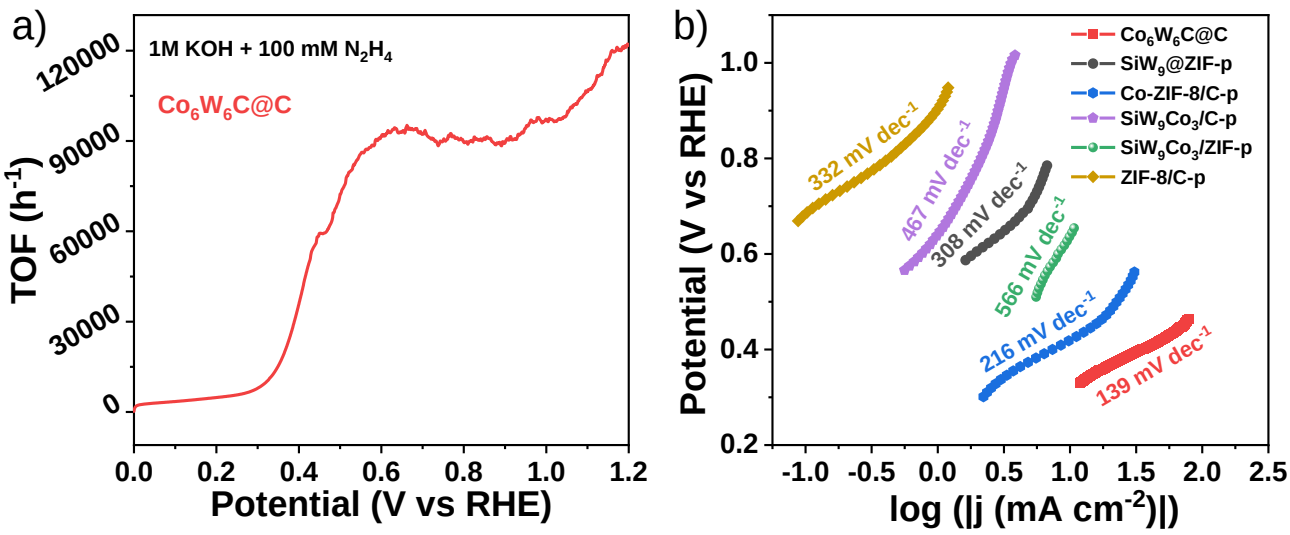

Fig. S12. a) The TOF of Co_6W_6C@C for HzOR. b) Tafel slope of different catalysts for HzOR.

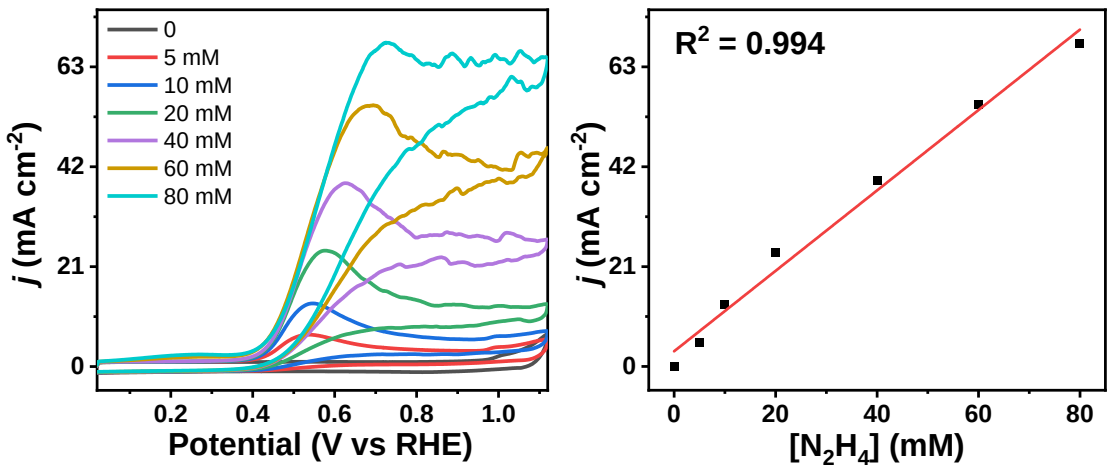

Fig. S13. a) CVs of Co_6W_6C@C in 1 M KOH solution with different N_2H_4 concentrations (scan rate of 5 mV s^{-1}). b) Relationship between the oxidation peak current densities and the N_2H_4 concentrations.

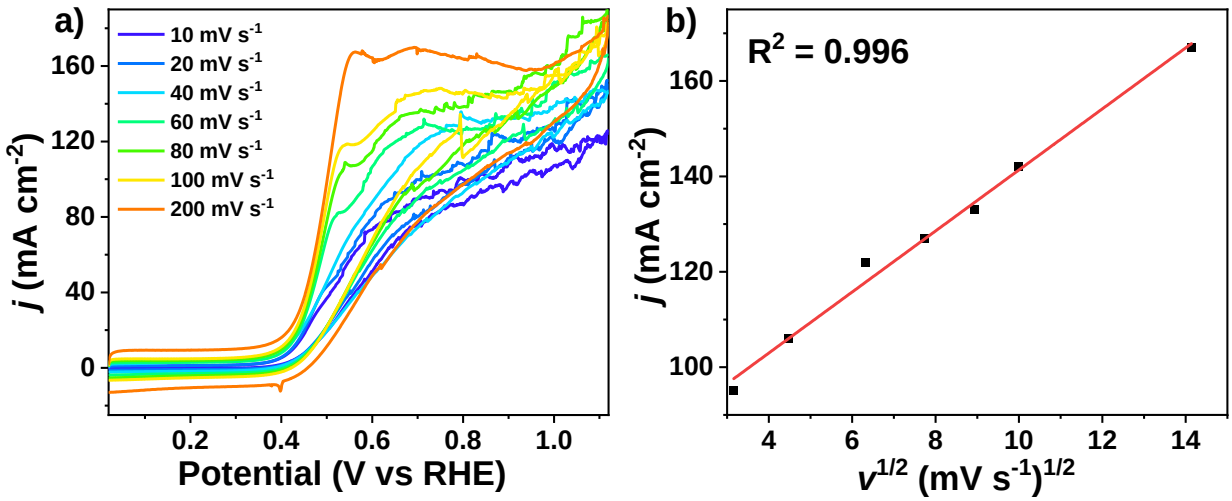

Fig S14. a) CVs of Co_6W_6C@C at different scan rates in 1 M KOH + 100 mM N_2H_4 solution. b) Relationship between the oxidation peak current densities and the $(\text{scanrate})^{1/2}$.

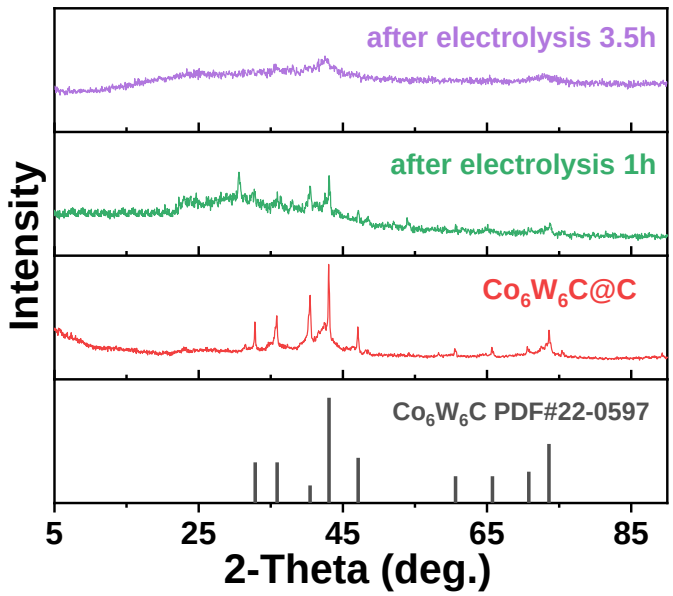

Fig S15. XRD patterns of Co_6W_6C@C before and after electrocatalysis.

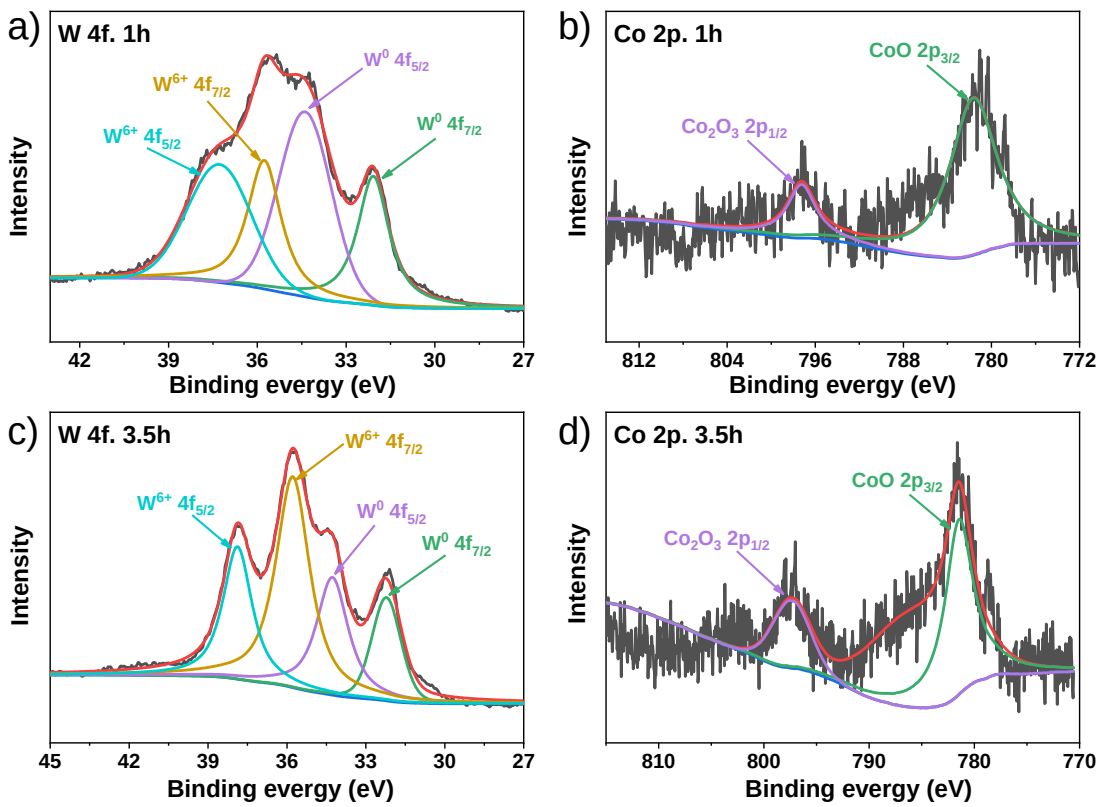

Fig S16. High-resolution W 4f and Co 2p XPS spectra of Co_6W_6C@C after 1 h and 3.5 h of electrocatalysis (applied potential fixed at 0.8 V vs RHE).

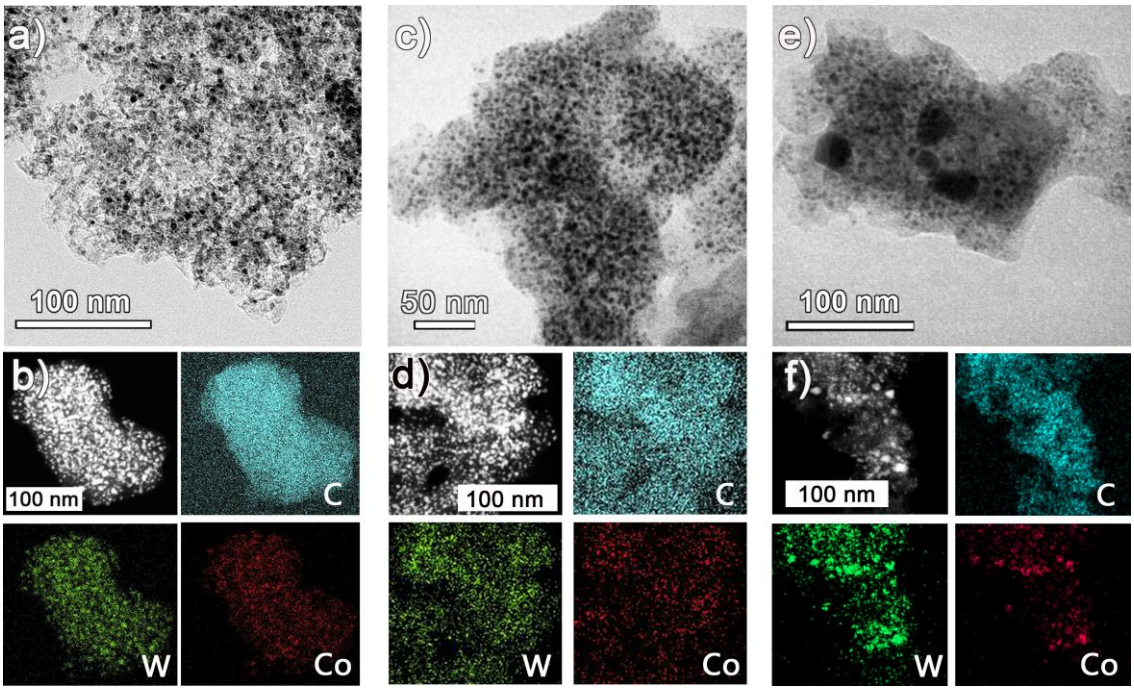

Fig S17. TEM images and EDX mapping of Co_6W_6C@C: a, b) as-synthesized, c, b) after electrolysis (1 h) and e, f) after 3.5 h of electrolysis (applied potential fixed at 0.8 V vs RHE).

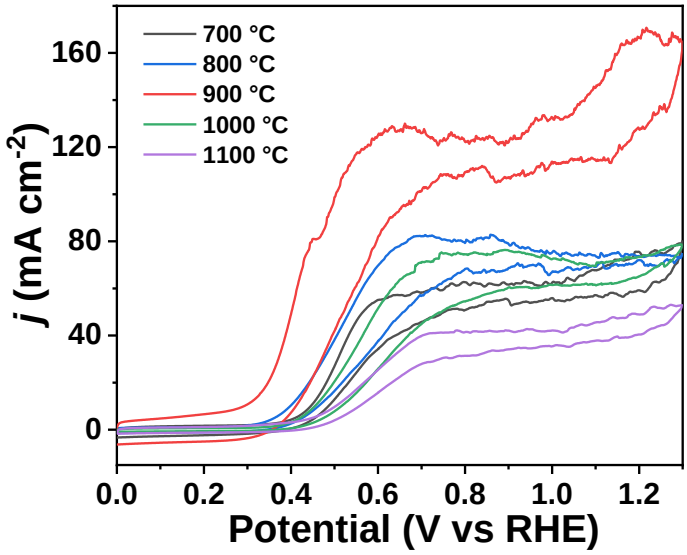

Fig S18. HzOR activities of the Co_6W_6C@C catalyst with different pyrolysis temperatures in 1 M KOH and 100 Mm N_2H_4 solution.

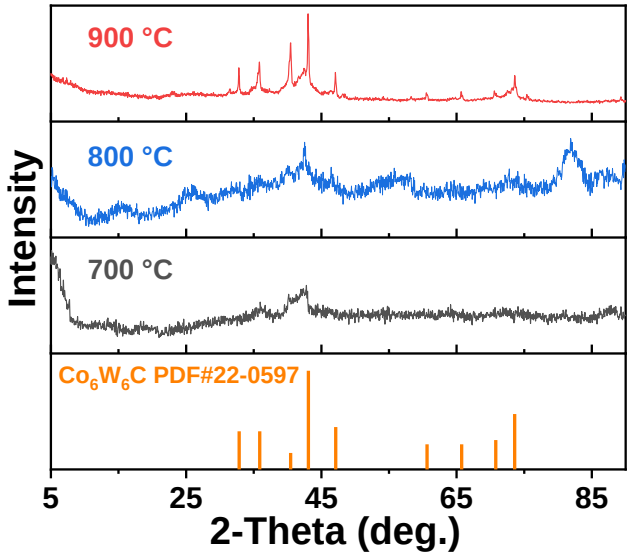

Fig S19. XRD patterns of pyrolyzed SiW_9Co_3@ZIF at 700°C, 800°C and 900°C.

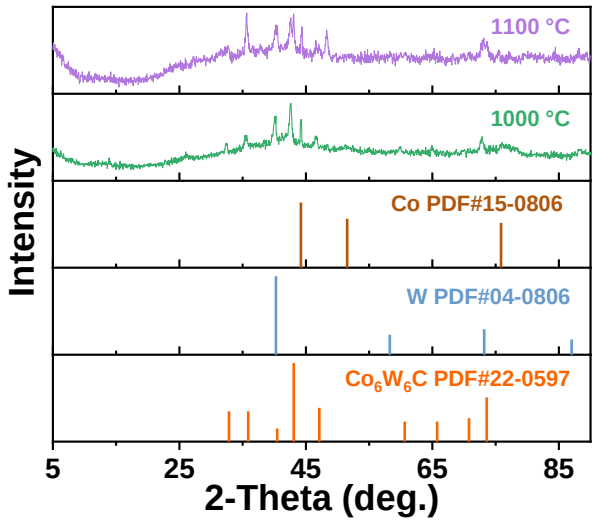

Fig S20. XRD patterns of pyrolyzed SiW_9Co_3@ZIF at 1000°C and 1100°C.

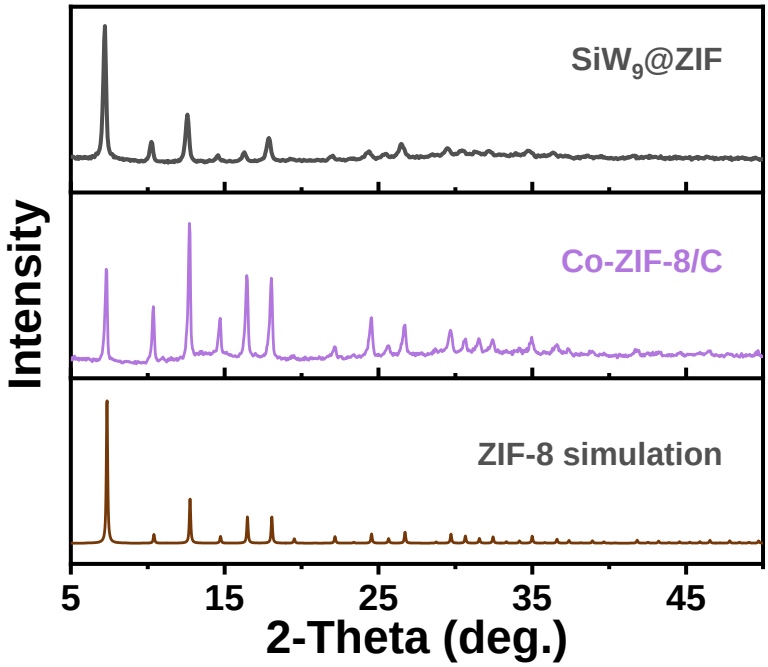

Fig. S21. XRD patterns of ZIF simulation, Co-ZIF-8/C and SiW_9@ZIF.

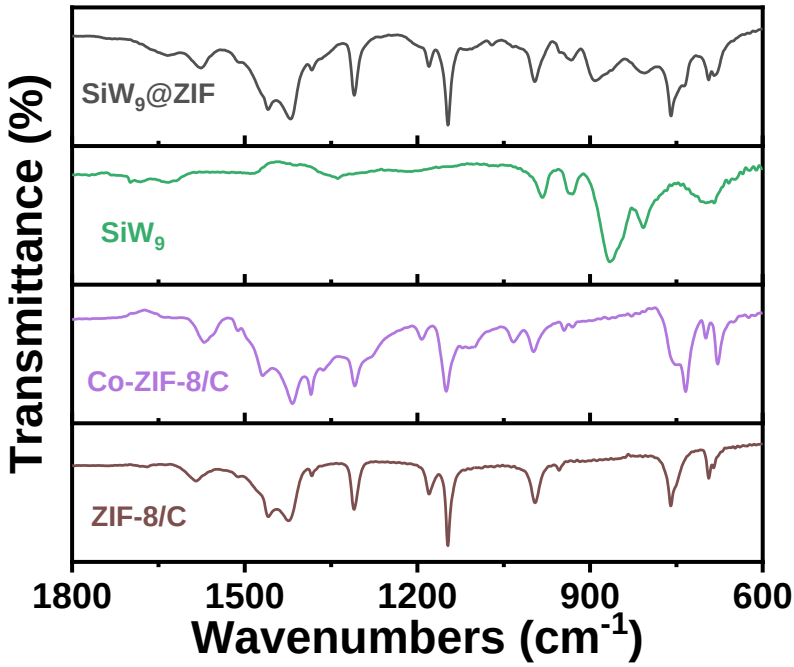

Fig. S22. IR spectra of ZIF-8/C, Co-ZIF-8/C, SiW_9 and SiW_9@ZIF

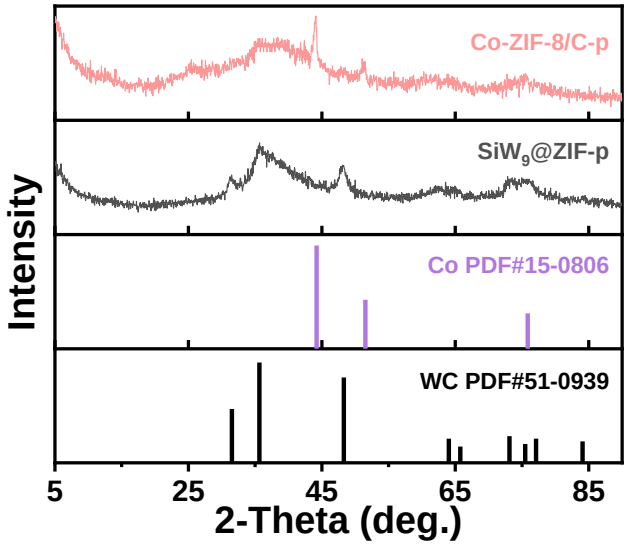

Fig. S23. XRD patterns of SiW_9@ZIF-p and Co-ZIF-8/C-p.

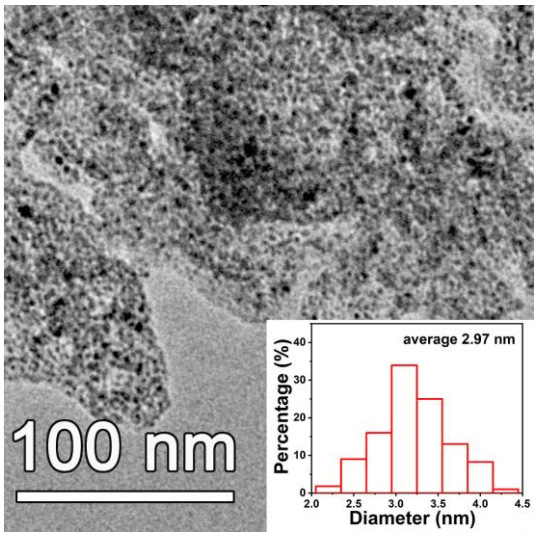

Fig. S24. TEM image of SiW_9@ZIF-p. (inset: particle size distribution of WC).

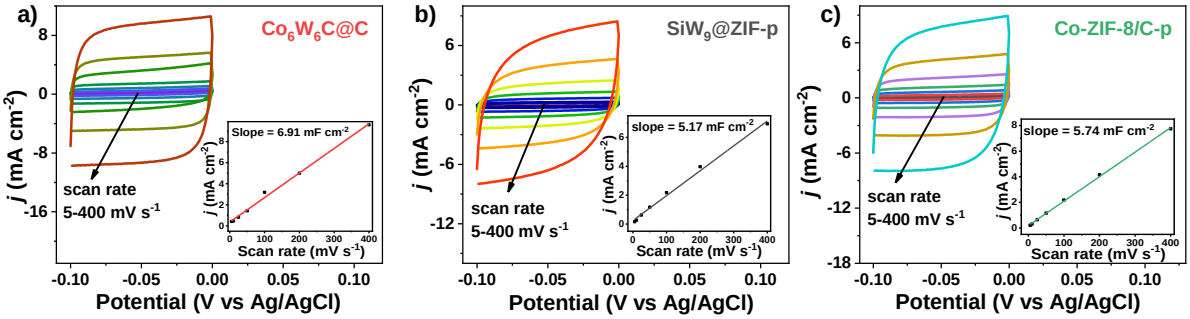

Fig. S25. CVs of a) Co_6W_6C@C, b) SiW_9@ZIF-p and c) Co-ZIF-8/C-p samples with different rates. (The capacitive current at -0.05 V as a function of scan rate for the corresponding samples.

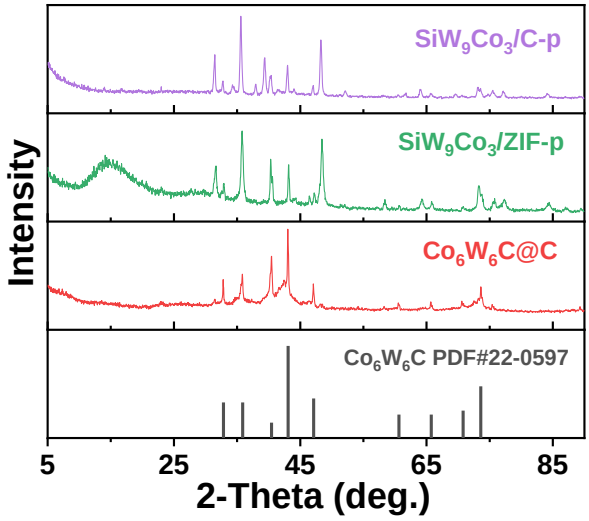

Fig. S26. XRD patterns of Co_6W_6C@C, SiW_9Co_3/ZIF-p and SiW_9Co_3/C-p.

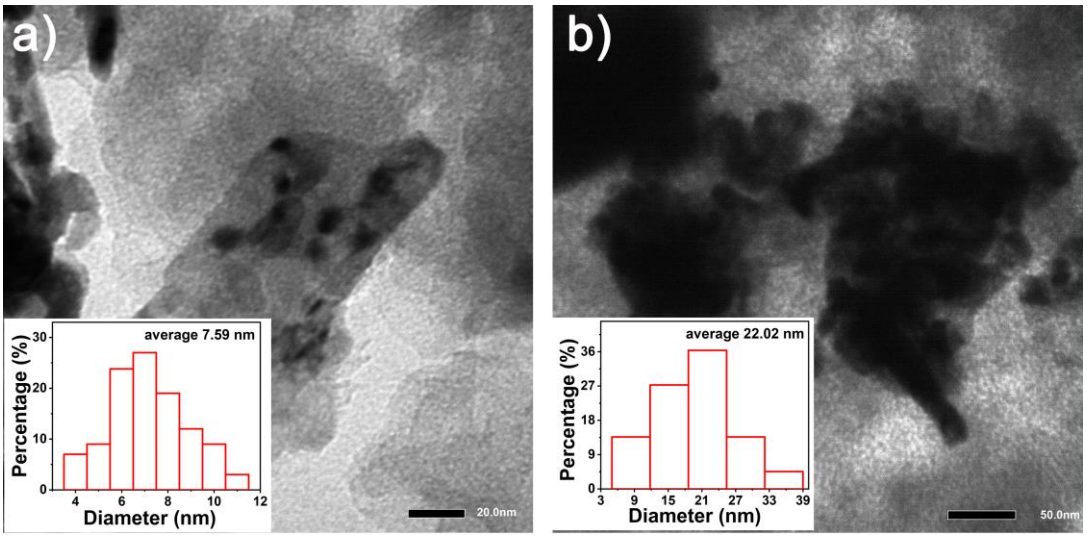

Fig. S27. TEM image of a) SiW_9Co_3/ZIF-p and b) SiW_9Co_3/C-p. (inset: particle size distribution)

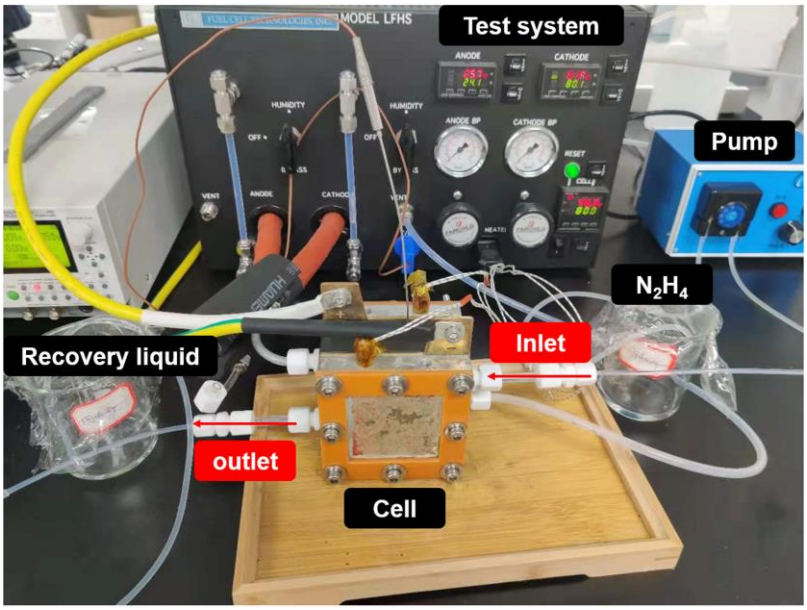

Fig. S28. Photograph of the setup for O_2-HzFC.

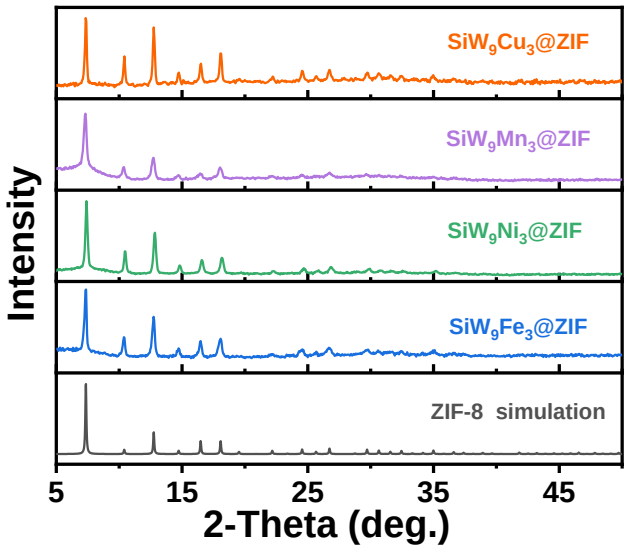

Fig. S29. XRD patterns of different SiW_9TM_3@ZIF (TM = Fe, Ni, Mn and Cu) samples.

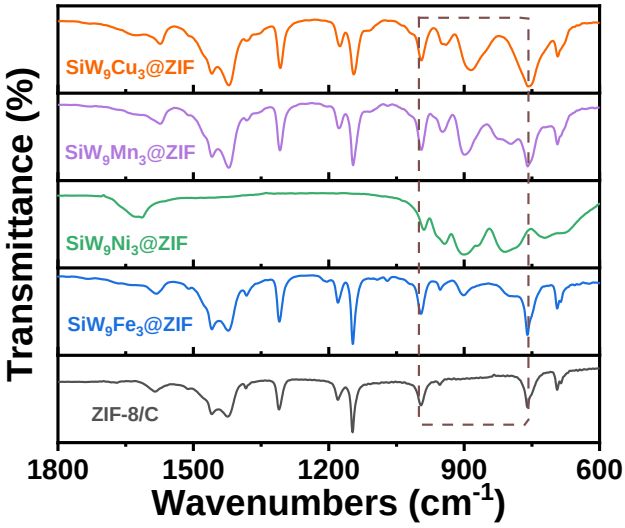

Fig. S30. IR spectra of different SiW_9TM_3@ZIF (TM = Fe, Ni, Mn and Cu) samples.

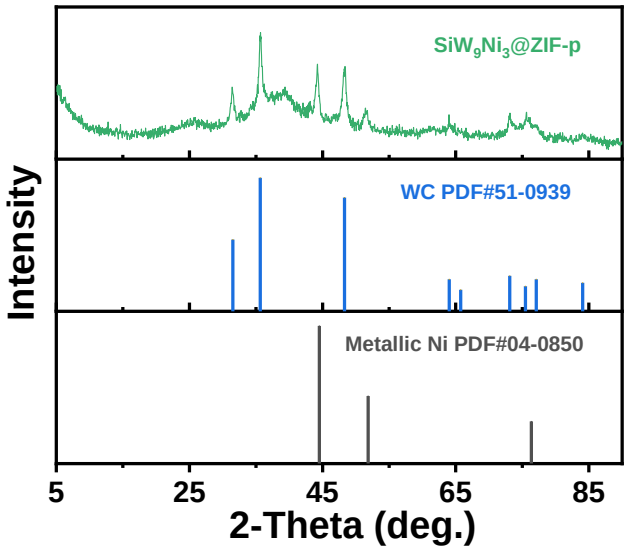

Fig S31. XRD pattern of SiW_9Ni_3@ZIF-p.

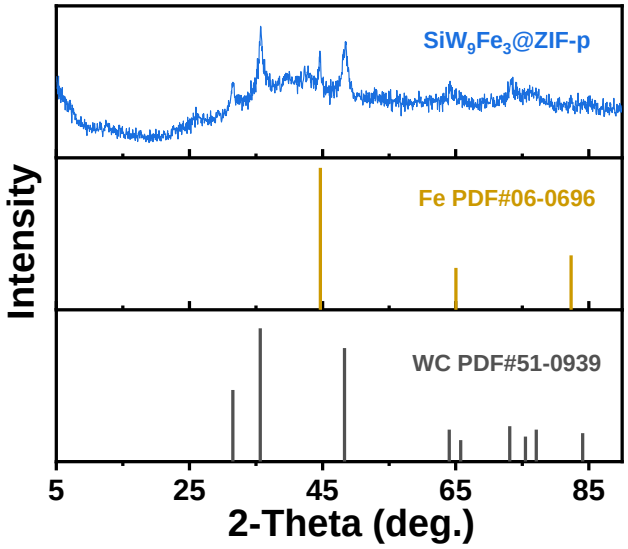

Fig S32. XRD pattern of SiW_9Fe_3@ZIF-p.

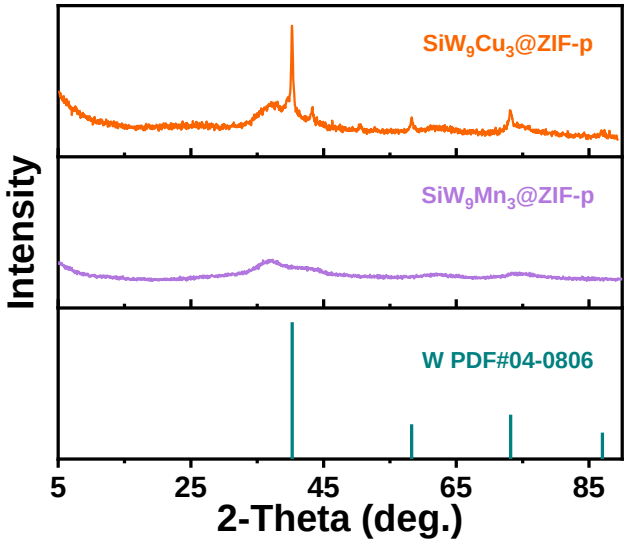

Fig. S33. XRD patterns of SiW_9Cu_3@ZIF-p and SiW_9Mn_3@ZIF-p.

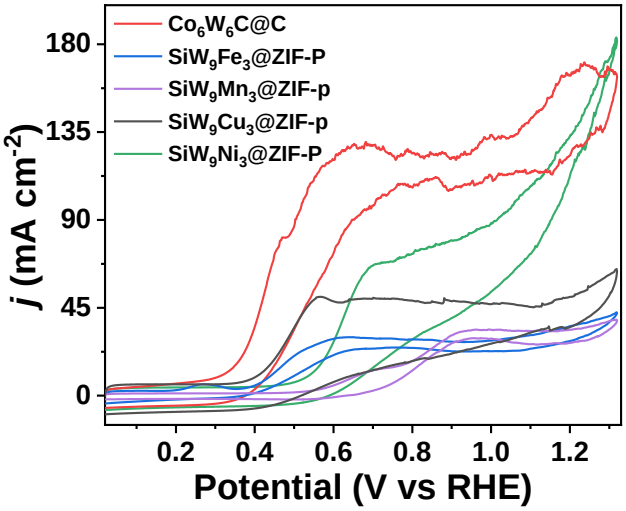

Fig. S34. HzOR catalytic activities of different SiW_9TM_3@ZIF-p in 1M KOH and 100 mM N_2H_4 solution.

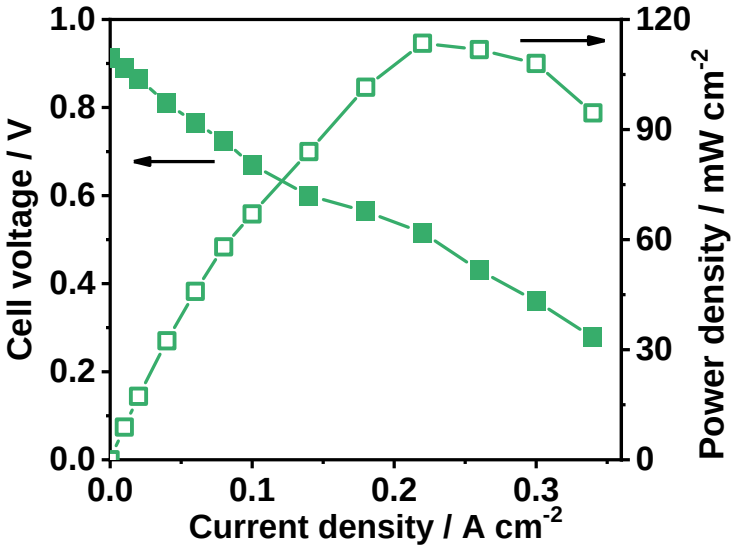

Fig S35. Polarization and power density plots for SiW_9Ni_3@ZIF-p at 80 °C. Testing conditions: the anolyte is 6.0 M KOH + 0.5 M hydrazine hydrate with a flow rate of 1 mL min^{-1}; the catholyte is O_2 with a flow rate of 0.2 L min^{-1}.

Table S1. The element analysis of as-synthesized samples

Samples	Atomic contents					
	C (wt %)	H (wt %)	N (wt %)	Zn (wt %)	W (wt %)	Co (wt %)
ZIF-8	47.63	6.27	22.71	22.98	—	—
ZIF-8/C	48.79	6.01	22.23	22.86	—	—
ZIF-8/C-p	80.72	1.31	17.21	—	—	—
SiW_9Co_3@ZIF	38.41	2.33	15.43	17.26	20.73	2.36
Co_6W_6C@C	40.12	1.29	0.62	—	42.20	12.78
Co_6W_6C@C after electrolysis 1h	47.32	1.01	0.51	—	33.16	7.31
Co_6W_6C@C after electrolysis 3.5h	68.25	1.11	0.59	—	12.05	5.52

Table S2. Comparison of activity and O_2-HzFCs performance between the Co_6W_6C@C and other HzOR catalysts reported in the literature [a].

Catalysts	Condition	Onset potential (V)[b]	Specific activity at E = 0.60 V (mA cm^{-2})	Peak specific activity (mA cm^{-2}) @potential (V vs RHE)	Peak mass activity (mA mg^{-1})	P_{max} (mW cm^{-2})[c]	Ref[d]
Co_6W_6C@C	**1M KOH + 100 mM N_2H_4**	**0.26**	**130**	**130@0.6**	**472**	**203**	**This work**
Co_3Ta	1M KOH + 100 mM N_2H_4	-0.086	n.m.	50@0.16	n.m.	n.m.	6
SeNCM	1M KOH + 100 mM N_2H_4	0.43	~20	30.8@0.8	n.m.	180	7
Ni_1Co_3	1M KOH + 100 mM N_2H_4	-0.15	~10	40@0.1	n.m.	n.m.	8
CaSC-Co^R	0.1M KOH + 50 mM N_2H_4	0.5 V	~1.2	3@0.9	n.m.	n.m.	9
Fe_2MoC	1M KOH + 100 mM N_2H_4	0.27	15	15@0.6	n.m.	n.m.	10
MoC_x	0.2M KOH + 10 mM N_2H_4	0.80	~1	8@1.2	n.m.	150	11
ZnO/SWCNT	0.1M NaOH + 1 mM N_2H_4	0.60	0	140@1.32	n.m.	n.m.	12
$Ni_{0.9}Co_{0.1}$-ANSA	3M NaOH + 0.5 M N_2H_4	-0.2	n.m.	280@0.15	n.m.	n.m.	13
Ni-Cu	3M NaOH + 0.1 M N_2H_4	-0.1	n.m.	340@0.45	n.m.	n.m.	14
Fe-CoS_2	1M KOH + 100 mM N_2H_4	0.15	n.m.	300@0.2	n.m.	125	15

Note: [a]HzOR, hydrazine oxidation reaction. Scan rate: 5-50 mV s^{-1}. [b]All potentials have been converted to RHE *via* the Nernst equation. [c] P_{max}: peak power density. [d] References: Ref. n.m.: not mentioned.

References

1 Y. Zheng, F. He, M. Chen, J. Zhang, G. Hu, D. Ma, J. Guo, H. Fan, W. Li and X. Hu, *ACS Appl. Mater. Interfaces*, 2020, **12**, 38183–38191.
2 Y. Wang, Q. Wang, L. Wan, Y. Han, Y. Hong, L. Huang, X. Yang, Y. Wang, K. Zaghib and Z. Zhou, *J. Colloid Interface Sci.*, 2020, **563**, 27–32.
3 Gilbert. Herve and Andre. Teze, *Inorg. Chem.*, 1977, **16**, 2115–2117.
4 J. L. F. Ortega, P. Sethuraman, D. E. Katsoulis, C. E. Costello and M. T. Pope, *J Chem Soc Dalton Trans*, 1992, 1901–1906.
5 J. Zhu, L. Qin, A. Uliana, J. Hou, J. Wang, Y. Zhang, X. Li, S. Yuan, J. Li, M. Tian, J. Lin and B. Van der Bruggen, *ACS Appl. Mater. Interfaces*, 2017, **9**, 1975–1986.
6 G. Feng, L. An, B. Li, Y. Zuo, J. Song, F. Ning, N. Jiang, X. Cheng, Y. Zhang and D. Xia, *Nat. Commun.*, 2019, **10**, 4514.
7 T. Wang, Q. Wang, Y. Wang, Y. Da, W. Zhou, Y. Shao, D. Li, S. Zhan, J. Yuan and H. Wang, *Angew Chem*, 2019, 7.
8 H. Wang, Y. Ma, R. Wang, J. Key, V. Linkov and S. Ji, *Chem. Commun.*, 2015, **51**, 3570–3573.
9 V. H. Fragal, E. H. Fragal, T. Zhang, X. Huang, T. S. P. Cellet, G. M. Pereira, A. Jitianu, A. F. Rubira, R. Silva and T. Asefa, *Adv. Funct. Mater.*, 2019, **29**, 1808486.
10 K. Ojha, E. M. Farber, T. Y. Burshtein and D. Eisenberg, *Angew. Chem. Int. Ed.*, 2018, **57**, 17168–17172.
11 J. Deng, X. Li, S. Imhanria, K. Chen, X. Deng and W. Wang, *Electrochimica Acta*, 2021, 138417.
12 K. N. Han, C. A. Li, M.-P. N. Bui, X.-H. Pham and G. H. Seong, *Chem Commun*, 2011, **47**, 938–940.
13 G. Feng, Y. Kuang, P. Li, N. Han, M. Sun, G. Zhang and X. Sun, *Adv. Sci.*, 2017, **4**, 1600179.
14 M. Sun, Z. Lu, L. Luo, Z. Chang and X. Sun, *Nanoscale*, 2016, **8**, 1479–1484.
15 X. Liu, J. He, S. Zhao, Y. Liu, Z. Zhao, J. Luo, G. Hu, X. Sun and Y. Ding, *Nat. Commun.*, 2018, **9**, 4365.